International Forum on Aeroelasticity and Structural Dynamics
IFASD 2017
25-28 June 2017 Como, Italy

STRUCTURAL DYNAMIC INFLUENCE OF AN UHBR ENGINE ON A COANDA-WING

T. S. Müller[1] **and H. Hennings**[1]

[1]German Aerospace Center (DLR), Institute of Aeroelasticity
Bunsenstrasse 10, 37073 Göttingen, Germany
T-SMueller@dlr.de, Holger.Hennings@dlr.de

Keywords: Multibody, Gyroscopic Moment, Eigen behavior, UHBR

Abstract:

Due to the need of higher efficiency and the reduction of CO_2 and noise emission the bypass ratio of gas turbines tends to increase. This leads to higher rotational masses which arises the question of gyroscopic moments influencing the eigenbehavior of the aircraft and thus the system stability regarding structural depended phenomena, e.g. flutter. Therefore this paper presents a multibody model to determine the structural coupling between a Coanda wing and an ultra high bypass ratio gas turbine (BPR of 17). The results in form of the spectral analysis of an eigenvalue analysis enables the understanding of the coupling mechanisms and gyroscopic influences. By analyzing the time dependent behavior of the wing-engine system under consideration of a follower force, representing the thrust, deepens the understanding of the structural load at the wing root.

1 INTRODUCTION

In the multidisciplinary framework of the Collaborative Research Center 880, consisting of the Technical University of Braunschweig, Leibniz University Hannover and the German Aerospace Center, a promising aircraft is developed according to the technology of 2030 [9]. The superordinate aim of the research is to combine high-lift technologies thus increasing the efficiency of point-to-point connections in major economic areas. Additionally, equal demands such as less fuel consumption and the reduction of the emission of CO_2 and noise are addressed. In order to achieve these goals and support the tendency towards greater bypass ratios, which can be historically foreseen by the engine manufacturers [10], a gas turbine with an ultra-high bypass ratio is to be used.

Furthermore the main priority in aircraft construction is to ensure the safety during flight against system instabilities e.g. flutter, which is a phenomenon based on the coupling of aerodynamic and structural forces. This aeroelastic instability is mainly influenced by structural characteristics of the aircraft structure. Under the assumption that the bypass ratio tends to increase in the future, the rotational masses increase, too. Whereby gyroscopic effects need to be considered [12]. Therefore a multibody model consisting of a Coanda wing from [11] and a UHBR engine from [8] was built up, to investigate the dynamical coupling of the engine-wing structure. The results improve the understanding of the given system and additionally give input for a reduced order model of the CRC 880 [5].

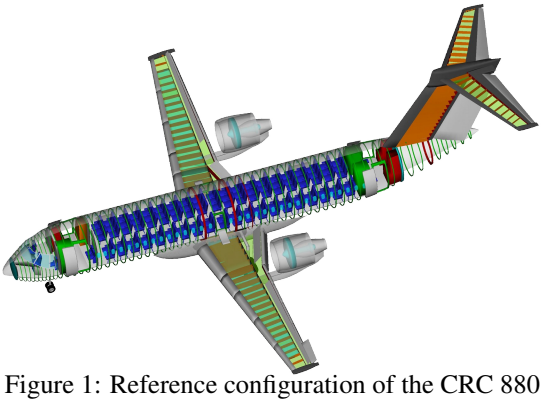

Figure 1: Reference configuration of the CRC 880

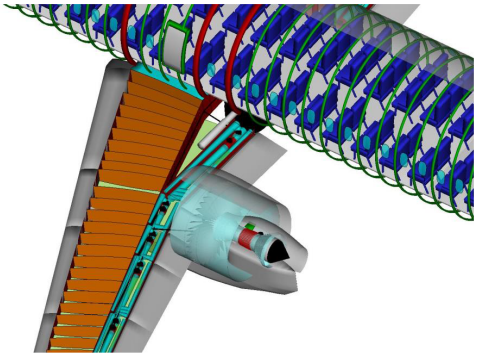

Figure 2: Close-up of the engine mounted over the Coanda-wing

A fundamental general investigation concerning the aeroelastic stability was performed for a free cantilevered wing by [4]. The principal influence on the eigenbehavior and thus on the system stability by placing a mass at the wing tip was analyzed by [7]. The results show a reduction in the flutter velocity. Additional investigations were carried out by [2, 3] concluding a high sensitivity of the dynamical aeroelastical characteristics of the wing towards the positioning of a mass connected to the wing. [1] investigated the influence of thrust in the form of a follower force under isolated conditions. Those numerical investigations used a finite element formulation whereas this paper uses a different approach using multibody dynamics capturing large deformations to conduct the yet neglected gyroscopical influences.

2 BASIC EQUATIONS

In the following chapter the governing equations describing the time variant influence of the angular momentum of a rotational shaft with a mounted disk, as a generic example for a gas turbine shaft, are presented.

2.1 Angular Momentum

To determine the angular momentum of a rotating system, more precisely of a rotating disc mounted on a shaft with the degree of freedom to tilt, it is described the easiest in a principal axis system (figure 3). Assuming rotational symmetry of the disc and the shaft, a rotational fixed coordinate system (x',y',z') is introduced. The x'-axis coincides with the symmetry axis of the disc and the y'- and z'-axis as center plane of the disc. Ω corresponds to the rotational velocity and w_s and v_s the translation of the center of gravity of the disc. φ_{ys} and φ_{zs} describe the tilting motion of the disc.

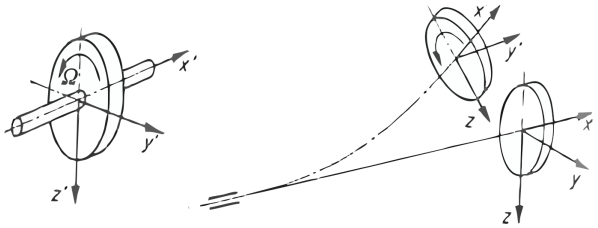

Figure 3: x', y', z'-principal axis exemplaric depicted at a rotationally symmetric disc.

Consequently the components of the angular momentum are states as followed ((1) ff.):

$$L_x = \theta_p \dot{\varphi}_{xs} \tag{1}$$
$$L_y = \theta_a \dot{\varphi}_{ys} \tag{2}$$
$$L_z = \theta_a \dot{\varphi}_{zs} \tag{3}$$

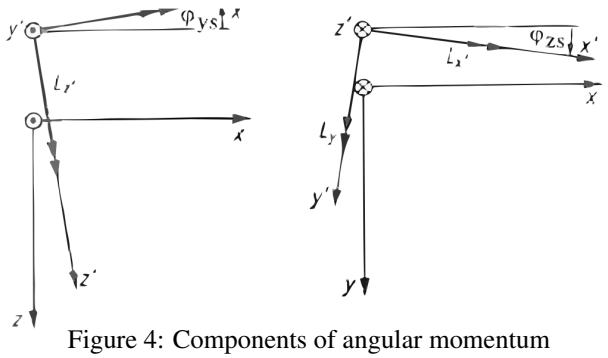

Figure 4: Components of angular momentum

The angles $\varphi_{xs}, \varphi_{ys}$ and φ_{zs} are the angles of the disc and θ_p and θ_a the polar, respectively the axial moments of inertia. Under the assumption of small angles, the component $L_x = -\Theta_p \Omega$ is constant due to the fact that $\Omega = \dot{\varphi}_{xs} = \text{const}$. This leads to the formulation of L_y(4) and L_z(5):

$$L_y = L_{y'} + L_{x'} \varphi_{zs} = \Theta_a \dot{\varphi}_{ys} - \Omega \Theta_p \varphi_{zs} \tag{4}$$
$$L_y = L_{z'} - L_{x'} \varphi_{ys} = \Theta_a \dot{\varphi}_{zs} + \Omega \Theta_p \varphi_{ys} \tag{5}$$

The resulting moment on the structure can be described as a time derivative of the rotational momentum (figure 4):

$$M_y = \dot{L}_y = \Theta_a \ddot{\varphi}_{ys} - \Omega \Theta_p \dot{\varphi}_{zs} \tag{6}$$
$$M_z = \dot{L}_z = \Theta_a \ddot{\varphi}_{zs} + \Omega \Theta_p \dot{\varphi}_{ys} \tag{7}$$

The terms $\Theta_a \ddot{\varphi}_{ys}$(6) and $\Theta_a \ddot{\varphi}_{zs}$ (7) correspond to the resulting moments due to the rotary inertia. Both, the terms $\Omega \Theta_p \dot{\varphi}_{zs}$ (6) and $\Omega \Theta_p \dot{\varphi}_{ys}$ (7) are the influences of the gyroscope.

2.2 Forward and Backward Whirl of a Rotating Shaft

The second phenomenon in context with the change of angular momentum is the whirl movement of the rotating shaft. If the rotor is set in motion, it tends to bend and follows an orbital motion due to the flexibility of the shaft. With the approach of

$$\begin{Bmatrix} r_0 \\ \varphi_0 \end{Bmatrix} = \begin{Bmatrix} \hat{r_0} \\ \hat{\varphi_0} \end{Bmatrix} e^{\lambda t} \quad \textbf{with } \lambda = j\omega \tag{8}$$

Under the assumption of a symmetrical setup for the rotor of figure 3, with the stiffness factors s_{ik} ($s_{12} = s_{21} = 0$) the homogeneous linear system of equation is stated as follow:

$$\begin{bmatrix} (-m\omega^2 + s_{11}) & 0 \\ 0 & (-\Theta_a\omega^2 + \Theta_p\Omega\omega + s_{22}) \end{bmatrix} \cdot \begin{Bmatrix} \hat{r}_0 \\ \hat{\varphi}_0 \end{Bmatrix} = 0 \tag{9}$$

Solving this system (9) leads to

$$\omega = \pm\sqrt{\frac{s_{11}}{m}} \tag{10}$$

for pure transverse movement and a just tilting movement

$$\omega = \frac{\Theta_p}{2\Theta_a}\Omega \pm \sqrt{(\frac{\Theta_p}{2\Theta_a}\Omega)^2 + \frac{s_{22}}{\Theta_a}} \tag{11}$$

which is dependent on the rotational velocity. Under the assumption, that the examined system is not symmetrical, as assumed in the simplifications, each of the eigenfrequencies is dependent on the rotational velocity and shows the splitting up of the eigenfrequencies.

3 NUMERICAL MULTIBODY MODEL

The numerical model was modelled with a substructure technique importing the flexible components from Ansys as modal reduced models. Principally two models were merged, both with similar approaches. The finite element wing model from [11] and the multibody engine model with the topology from [8].

3.1 Engine Model

The geometry and geometrical parameters for the engine model are derived from Gasturb 12 [6] by meeting the flight conditions for [9]. Consequently the model consists of the nacelle (figure 5) and the drive shafts, consisting of three components (figure 6). The high pressure shaft consists of 8 compressor stages and 2 turbine stages. The low pressure shaft contains three booster stages and 4 turbine stages. The fan, connected with the low pressure shaft via a planetary gear, is reduced in rotational speed by a transmission ratio of 3.15. The direction of the rotational velocity of both units are consensual, whereas the high pressure shafts rotates in opposite direction with a factor of -1.43 compared to the rotational velocity of the low pressure shaft.

3.2 Wing Model

The geometrical dimensions for numerical model of the wing structure is depicted in figure 7. As reference configuration, the simulations were performed for the wing with flaps up. The geometrical parameters are listed in table 2. The pylon connection between the engine and the wing is assumed to be rigid.

The engine axis is mounted 4.51 m in span wise direction from the aircraft axis (y-direction), 1.57 m over the middle axis of the wing (z-direction) and the inlet of the engine nacelle is located at 5.301 m with respect to depicted inertial system (figure 8).

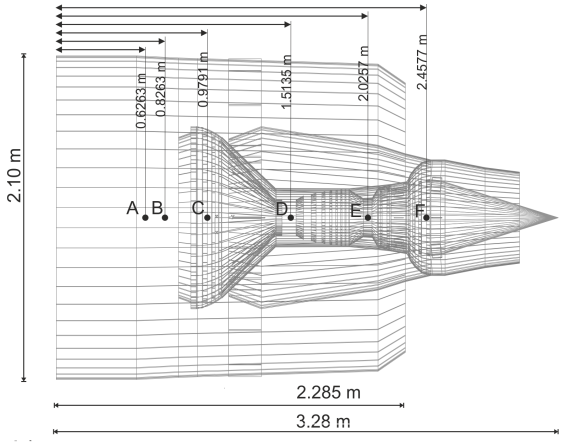

Figure 5: Sectional drawing of the UHBR nacelle

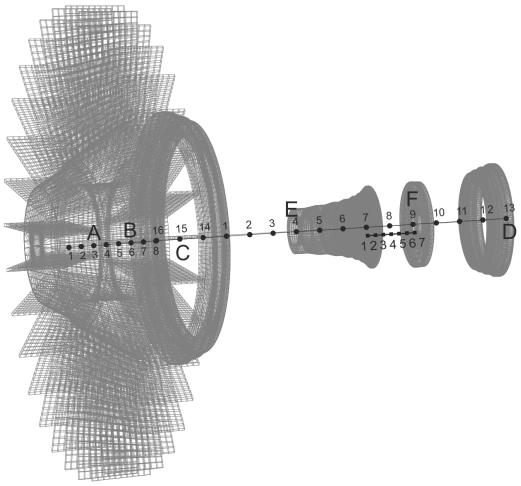

Figure 6: Multibody model of the UHBR gas turbine

Table 1: Eigenfrequencies of the wing. (B.=Bending, T.=Torsion, In.=Inplane, A.=Axial)

Mode No.	f_0 **[Hz]**	**Mode Shape**	**Mode No.**	f_0 **[Hz]**	**Mode Shape**
1	24.18	B. LP	6	153.11	B. Fan
2	61.04	B. Fan	7	189.43	A. LP
3	103.97	B. LP	8	375.84	B. LP
4	106.89	A. Fan	9	408.59	T. Fan
5	144.47	A. HP	10	445.66	B. HP

Table 2: Geometrical details of the wing

Reference Area	$\sim 45m^2$
Aspect Ratio	8.35
Sweep Angle	26°
25% Chord Sweep Angle	20.7°/ 23.3°
Max. t/c Ratio	13.5/13.5/12.75/10.3

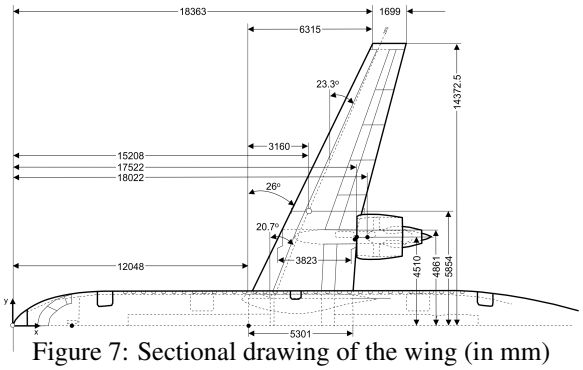

Figure 7: Sectional drawing of the wing (in mm)

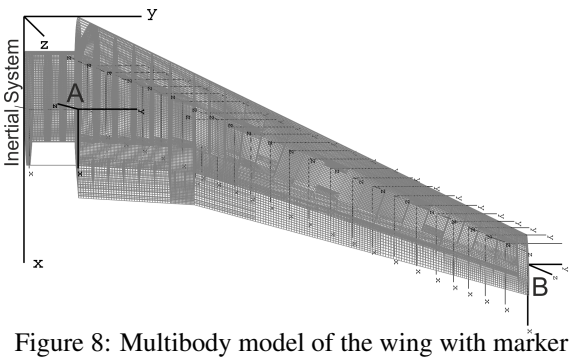

Figure 8: Multibody model of the wing with marker

Table 3: Eigenfrequencies of the wing. (B.=Bending, T.=Torsion, In.=Inplane, E. = Engine)

	Clean Wing		**Wing+Engine (Masspoint)**		**Wing+Engine (MBS-Model)**	
Mode No.	f_0 **[Hz]**	**Mode Shape**	f_0 **[Hz]**	**Mode Shape**	f_0 **[Hz]**	**Mode Shape**
1	2.56	B.	1.77	B.	1.77	B.
2	8.31	In.-B.	3.17	B.	3.17	B.
3	9.32	B.	5.19	In.-B.	5.18	In.-B.
4	9.46	In.-B.	10.49	In.-B.	10.49	In.-B.
5	9.52	B.	15.97	In.-B.	15.96	In.-B.
6	21.12	B.	19.15	In.-B.	19.10	B.-T.
7	23.26	T.	27.87	T.	24.18	E. B.
8	32.33	In.-B.	29.58	B.-T.	24.22	E. B.
9	37.96	B.	38.45	B.	27.86	T.
10	42.03	T.	38.90	B.	33.96	B.-T.

In order to achieve the given physical characteristics of the finite element model of the eigenvalue analysis, the wing was modal reduced with 30 master nodes as static modes and additional 10 dynamical modes were extracted. Whereby only the first 40 modes, with a representative frequency range up to 100 Hz, were used in the multibody description.

The eigenvalues for the the different versions *clean wing (no engine)*, *wing with engine (as masspoint)* and *wing with engine (modelled as mbs)* are listed in table 3. Not only the eigenfrequencies itself change crucially by considering an additional body afflicted by mass and inertia, but also the modeshapes change from mainly bending to in plane and torsion motions. In the next step a more complex model of the engine [8] is considered. Around the first frequency of the engine, the frequencies of the wing tend to change, presumably resulting from a coupling of the engine model.

4 SIMULATION AND RESULTS

To determine the principal change in eigenbehavior of the wing structure and its coupling with the UHBR gas turbine several simulations were performed. Starting with the dependency of the eigenfrequeny to the rotational velocity Ω, in form a Campbell diagram, the angular momentum of the engine was varied by varying the gear ratio, followed by the comparison of a inversed angular momentum. Finally presenting the time dependent behavior under consideration of thrust in case of the design point: top of climb.

4.1 Campbell Diagram

In order to evaluate the principal influences and the gyroscopic coupling mechanism of a flexible wing and a flexible rotating drive train, a sensitivity analysis by increasing the rotational velocity with regard to the eingevalues of the model was performed. Two settings were simulated, the first one with a flexible wing structure but no modal respresentation for the gas turbine (figure 9). The second simulation was performed with both models considered as flexible bodies (figure 10). For the rigid engine model no change in the eigenbehavior of the wing was detected.

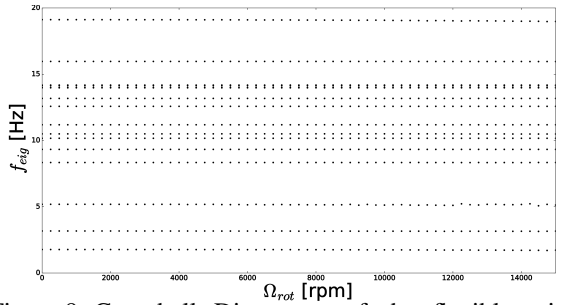

Figure 9: Campbell Diagramm of the flexible wing model and rigid UHBR engine model

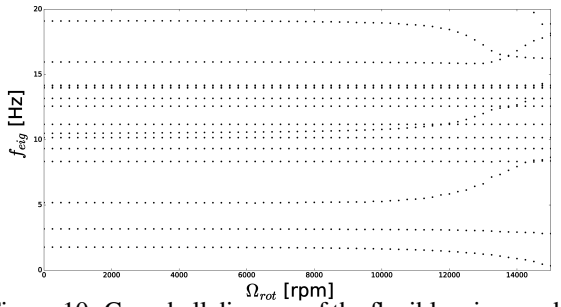

Figure 10: Campbell diagram of the flexible wing model and flexible UHBR engine model

Opposingly, the eigenfrequencies of the flexible engine model change in each mode shape of the wing in which a common movement of the wing and engine occurs (table 3). As expected, the higher the rotational speed and thus the angular momentum, the stronger the influencial change in the eigenbehavior. For the 1st, 2nd and 6th eigenfrequency decreases, whereas the 3rd, 4th and 5th eigenfrequency increases with increasing rotational velocity. This effect arises around 10000 rpm. The system shows a strong sensitivity, whereby this statement is relativized when considering the designpoint to be around $\sim$8000 rpm. The remaining constant eigenfrequencies are local oscillations, which have no participation in mode shapes, which are characterized by a global wing movement and thus not influenced by gyroscopic moments.

4.2 Influence of Angular Momentum

Since the principle influence of the coupling of both structures could be ascertained the main question is the influence of angular momentum on the structural behavior. As bypass ratios tend to increase in future times, a major challenge is the fan blade tip velocity. Exceeding of the rotational velocity over the threshold of Ma=1 leads to pressure surges and consequently to losses in performance. Therefore UHBR engines are equipped with an planetary gear decreasing the rotational velocity of the fan.

To determine the influence of the angular momentum, the gear ratio and the direction of the angular momentum are varied. As reference parameters the gear ratio is, as stated above, 3.15 and the reference direction is in positive y-direction (figure 8). Compared by the pure geometrical parameters the fan has a 4.6 times higher inertia than the low-pressure unit and a 98.6 times higher one than the high-pressure unit. The gear ratios were correspondingly varied :$\pm 30\%$ and $\pm 50\%$. Thus only the smallest ratio has a lower angular momentum than the low-pressure unit. The remaining ratios can be taken from figure 11.

Decreasing the gear ratio and thus increasing the rotational velocity of the fan leads to a reduction of the first four eigenfrequencies of the wing. The higher angular momentum leads to a smaller movement, respectively tilting of the UHBR gas turbine participating in the common mode shapes with the wing. This causes the wing mode shape to become pure bending/in plane mode shapes.

Inreasing the gear ratio and thus decreasing the rotational velocity of the fan impacts the eigenbehavior of the coupled system only marginally. The third eigenfrequency shows a small tendency the higher the frequencies becomes with respect to a higher gear ratio. Both behaviors can be traced back to the intrinsic behavior of the angular momentum to keep its direction and stabilizes itself. The smaller the angular momentum the easier it is to change its direction and vice versa.

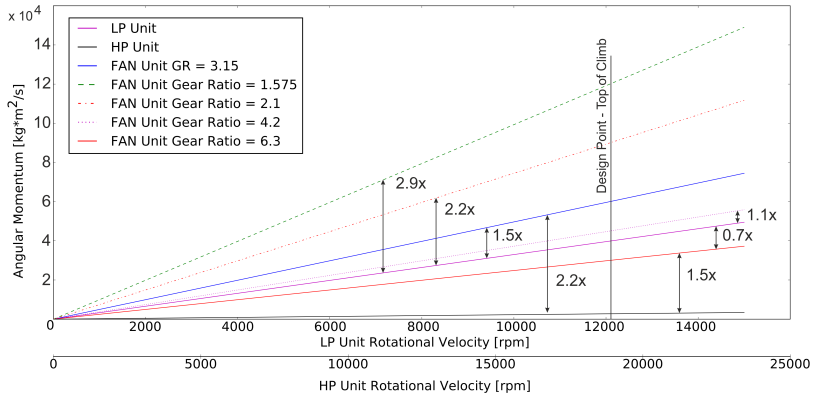

Figure 11: Comparison of the angular momentum by components over the rotational velocity and transmission ratio.

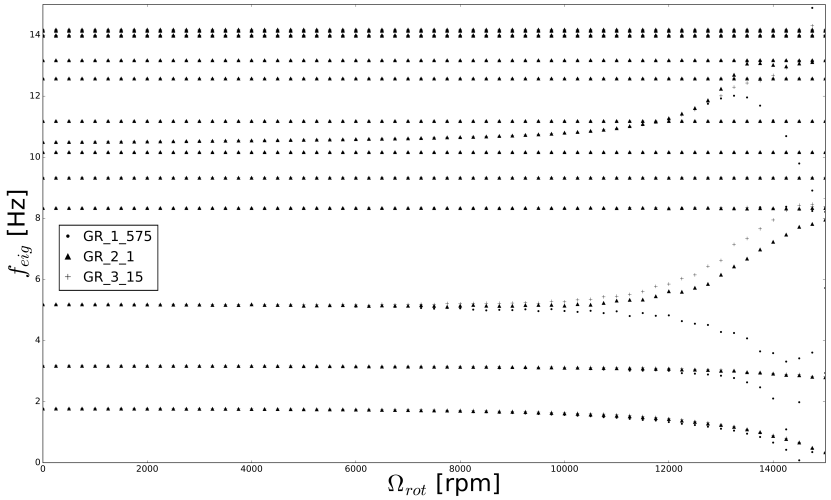

Figure 12: Campbell Diagram of the wing by increasing transmission ratio.

4.3 Linear System Analysis (LSA) - Wing Tip Excitation

To determine the forces and vibrations to be absorbed at the root of the wing (figure 8), the constraint forces in z-direction at the point **A** due to an harmonic sweep excitation in z-direction at the point **B**, at the tip of the wing, are evaluated. The excitation force has an amplitude of 0.5 m and a frequency range from 1 Hz to 250 Hz divided into 1000 sub steps.

The varying parameters of the LSA are the rotational velocity, the gear ratio and the frequency of a harmonic force acting upon the wing tip in z-direction.

4.3.1 Reference Configuration - Gear Ratio = 3.15

In order to determine the influence of the dynamics of the UHBR engine on the coupled system, the behavior of the turbine itself was first analyzed. For this purpose, the bearing forces of the fan (**A**), low-pressure shaft (**C**) and high-pressure shaft (**D**) due to the excitation force were evaluated.

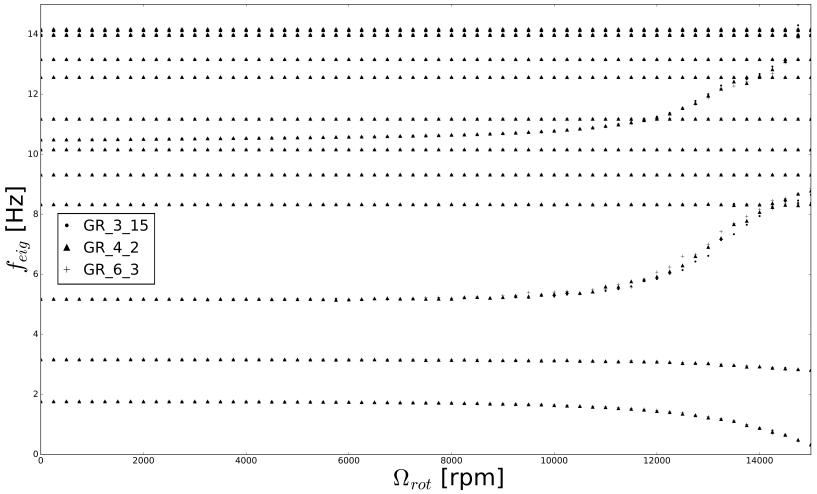

Figure 13: Campbell Diagram of the wing by decreasing transmission ratio.

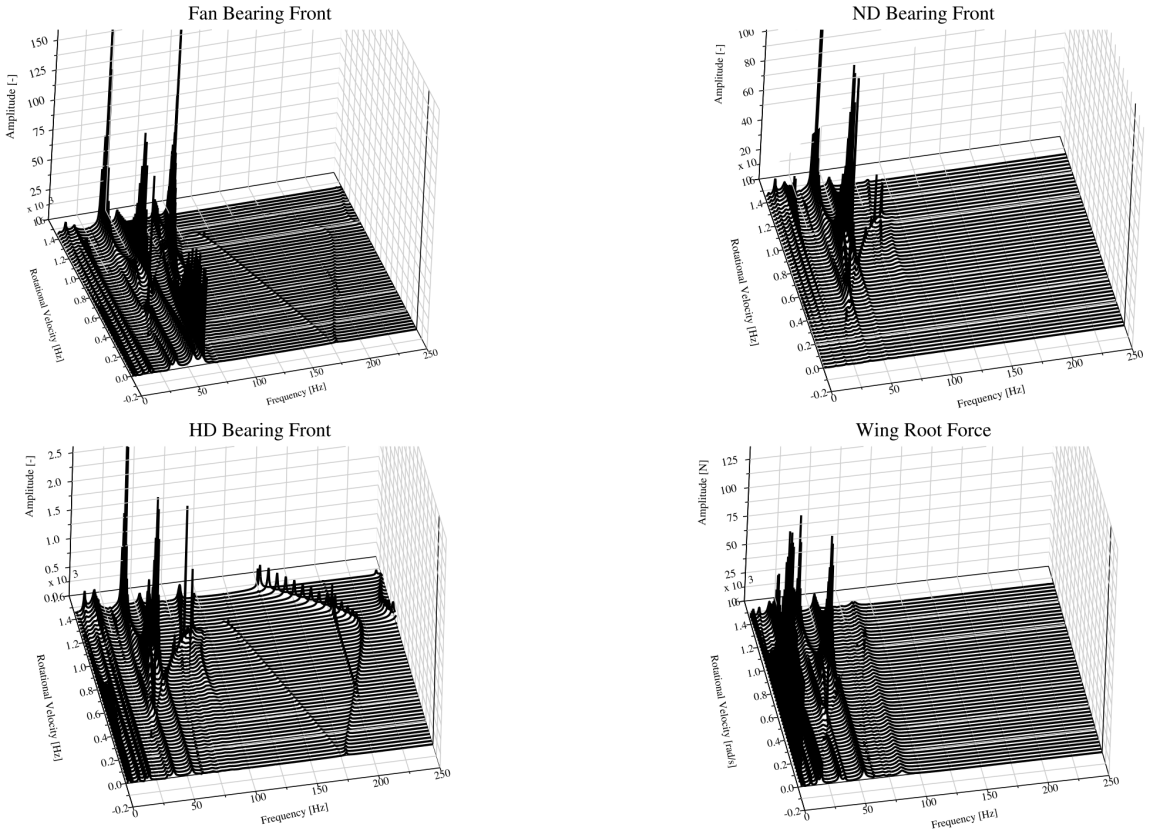

Figure 14: Campbell Diagram from different components of the model. Gear Ratio = 3.15

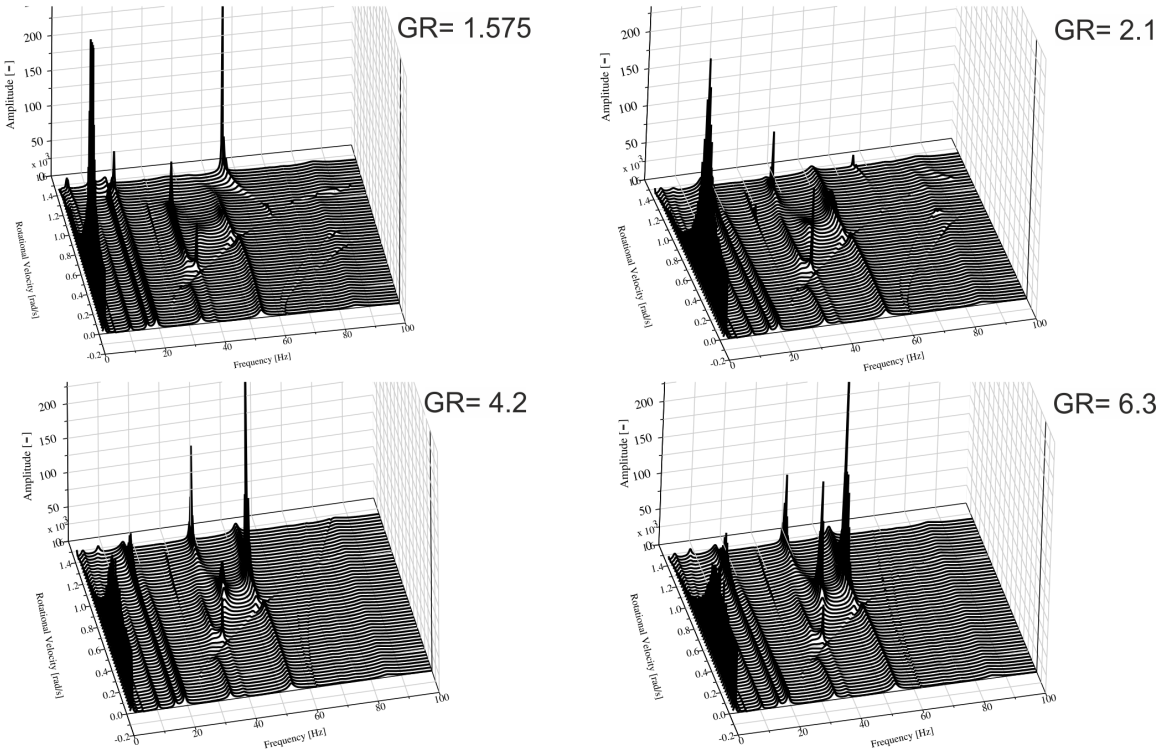

Figure 15: Campbell Diagram with varying gear ratio

The results for the LSA are depicted in figure 14 for the above mentioned output points. Principally two effects can be observed, on the one hand the excitation of the structure due to the external excitation force and on the other hand the coupling of eigenfrequencies causing a peak in the amplitude.

The first peak of the wing structure around 1.7 Hz, in the range up to 400 rad/s, is a bending mode excited from the external force. Coincidently the fan shaft is excited, at 62 Hz, due to its coupling with the excited bending mode. A significant phenomenon is the splitting of the eigenfrequencies of the rotating shafts (11). The shaft's tilting causes a change in the direction of the angular momentum and thus induces a moment softening/stiffening the structure. The splitting of the eigenfrequencies enables a coupling through the crossing with other eigenfrequencies. This can be illustrated clearly for the fan shaft starting at $\sim$176Hz. The double crossing of the forward-tilting mode with a eigenfrequency of the wing around 200Hz raises their amplitudes for the intersection point. This phenomenon is the reason for both the amplitudes around 37Hz (520 rad/s), 51Hz (1000 rad/s) and the two peaks around 80Hz (1150 rad/s). Those intersecting eigenfrequencies and the increase in their amplitude are transferred throughout the whole structure to the root of the wing.

4.3.2 Variation of the Gear Ratio

The influence of in-/decreasing angular momentum was analyzed by solely varying the gear ratio, thus the angular momentum is only changed by the fan dynamics. Thus for the eigenfrequencies of the fan the splitting decreased by increasing and increased by decreasing gear ratio. Thus there was no interaction with frequencies lower than 100Hz, which is why the diagram are only plotted up to this value. Over 100Hz the amplitudes are negligibly small. All other parameters have been copied from the previous settings. The results are show in figure 15.

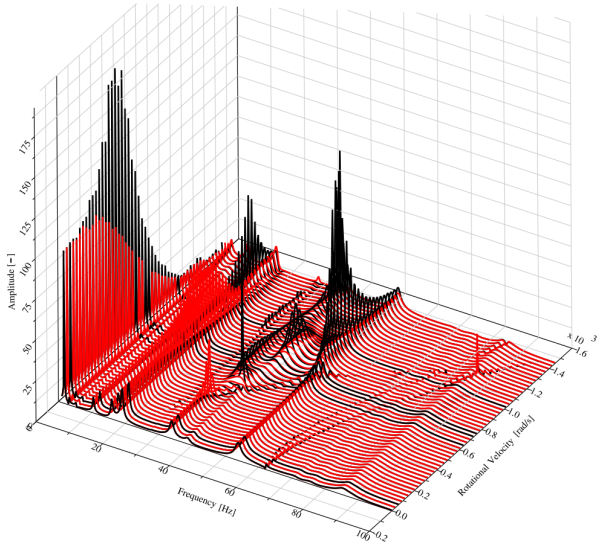

Figure 16: Campbell Diagram, comparison of opposite direction of angular momentum, GR = 3.15

Four different gear ratios, 1.575, 2.1, 4.2 and 6.3 were compared with the reference ratio of 3.15. With the lowest gear ratio, the fan occupies the highest angular momentum and vice versa. All four gear ratios show a peak around 1.7Hz, which corresponds to the first bending mode of the wing (see table 1 and section 4.3.1).

With increasing gear ratio this amplitude of the peak shrinks as the angular momentum decreases. Diametrically the amplitudes with higher frequency tend to increase with increasing gear ratio (decreasing angular momentum). The exception is the peak at ∼57Hz which corresponds to a mode shape including a strong orbital tilting of the UHBR engine. Decreasing the angular momentum leads to the increasing dominance of the coupling of the low-pressure unit and its frequency spectra.

4.3.3 Inversion of the Angular Momentum

Since the rotational direction of the gas turbine is not of necessity standardized, its reversal in the opposing direction is discussed in this section. The eigenfrequencies and behavior of the engine characteristics itself are not affected by the inversion of the angular momentum due to the fact that it is a structural characteristic whereas the dynamical parameters are held constant.

This statement is only valid and reasonable if the engine is treated isolated. Changing the direction of the angular momentum changes the algebraic sign in (6) and (7) but since the wing-engine system is not symmetrical one cannot assume a diametrical behavior of the system deriving its properties by reversing them.

For the analysis of the influence of the rotational momentum direction, the force on the wing root in the z direction is considered, as in the past sections. For the reference direction (’black’) in positive x-direction 7 significant peaks are detected at 1.74Hz (up to 1000 rad/s), 15.95Hz (around 1200 rad/s), 37.63Hz (at 522 rad/s and 1392 rad/s), 41.87Hz and 51.34Hz (870 rad/s) and 51.09Hz (at 986 rad/s) (figure 16). Changing the direction of the resulting angular momentum to the opposing direction (’red’) leads to only 4 remarkable eigenfrequencies, which are at 19.19Hz (696 rad/s), 33.65Hz (348 rad/s) and 86.49Hz at 1160 rad/s. Wherein additionally the amplitudes of the peak are significantly lower compared to the occurring maxima of the reference.

4.3.4 Variation of the Gear Ratio with Reversed Direction of the Angular Momentum

Reversing the resulting angular momentum of the engine decreases, in this case, nearly all significant amplitudes of the excited frequencies of the wing structure. As in section 4.3.2 mentioned: increasing the gear ratio from 1.575 to 6.3 the influence of the fan angular momentum decreases and thus the only influencing factor is the eigenbehavior of the low-pressure unit (figure 15 can be noticed), since the angular momentum of the high pressure unit is nearly negligible. In the case of the reversed angular momentum decreasing the angular momentum of the fan leads to decreasing amplitudes. Additionally it leaves the low-pressure unit again as the dominant influencial factor. However it is much more beneficial for the whole structure as the reference configuration.

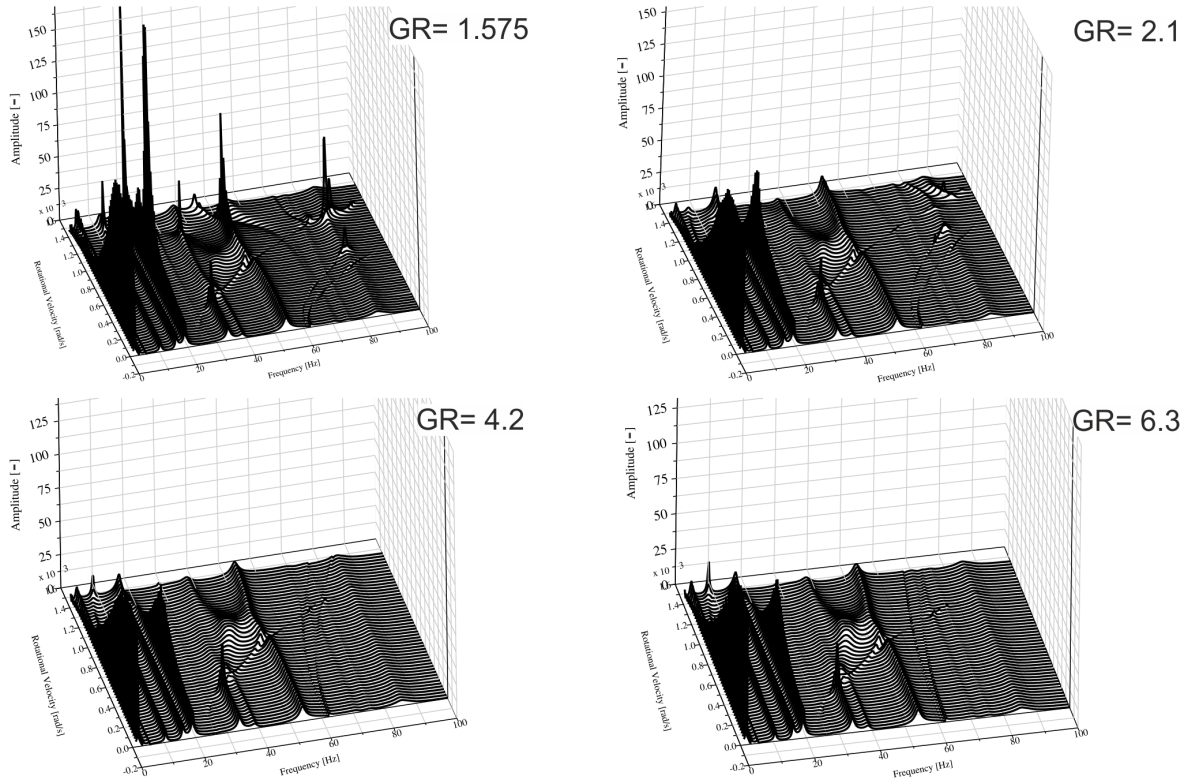

Figure 17: Campbell Diagram with varying gear ratio, angular momentum in opposite direction to reference

4.4 Time Dependent Behavior

To analyze possible non-linear/time dependent and evaluate the system behavior in the chosen design point, a time simulation was performed for the engine operating around the top of climb. Therefore the rotational velocities were embedded as boundary conditions (figure 11, $F_{Thrust} = 18.7$kN). The simulation ran for 100s to ensure a state of equilibrium, followed by a 100s interval representing the time dependent behavior.

Four different cases were simulated: the reference and the reversed angular momentum configuration, each with and without thrust. The thrust was modelled as a follower force (aligned with the axis of the gas turbine) acting on each stage of the UHBR gas turbine components where thrust is generated.

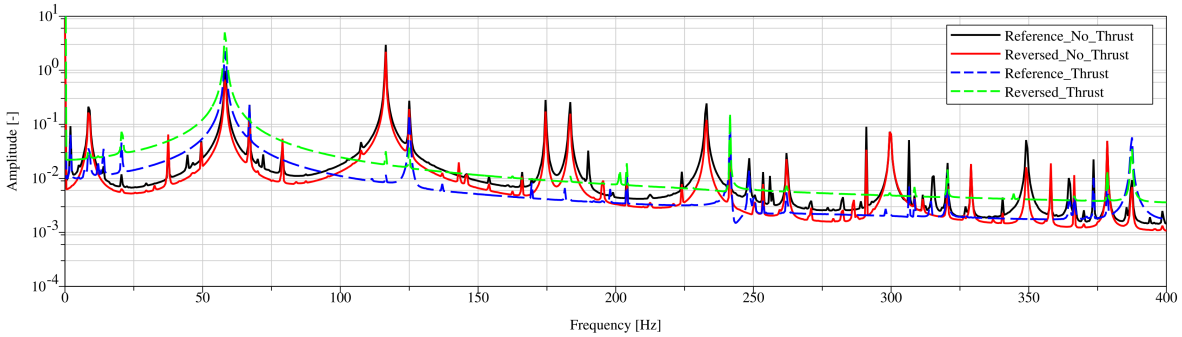

Figure 18: Frequency spectrum of the force at the wing root (Joint of the multibody model)

The results of the simulation are depicted in figure 18 in form of the RMS frequency spectrum. In comparison for the case of *no thrust* the basis level of the amplitude is slightly higher for the reference case. The structural behavior coincides in the majorly dominating peaks (8.5Hz, 58Hz, 116.5Hz, 125Hz, 174.5Hz, 183.5Hz, 233Hz).

Additionally several frequencies are exclusively excited compared to the reversed angular momentum (e.g. the peaks at 2Hz, 44.5 Hz, 72 Hz and 190 Hz). Preloading the wing with a force representing thrust , pre-stresses the wing however no general statement of the eigenfrequencies to in- or decrease can be made, since the wing is strongly asymmetrical. Prestressing the wing, on the one hand, causes throughout the whole spectrum smaller excitations to vanish, whereas the same trend of exclusive excitation being valid in these two cases, as in the cases just presented. On the other hand the basis amplitude level is higher up to 100Hz compared to *no thrust*. Further reversing the angular momentum causes a significant increase in the basis level of the amplitude compared to the reference.

5 CONLCUSION

This paper presented a multibody approach for the structural and dynamical coupling between a Coanda wing and an UHBR gas turbine. The results of the eigenvalue analysis could show the need to model the intrinsic eigenbehavior of the engine, due to a strong dependency and thus sensitivity to the rotational velocity of the rotating engine parts. Furthermore the gear ratio and thus the angular momentum is a sensitive parameter with regard to the system characteristics. Regarding the eigenbehavior, the fan unit dominates the lower frequencies ($\leq$25Hz), whereas the low-pressure unit influences frequencies $\geq$25Hz. Reversing the resulting angular momentum in opposing direction changes the structural loads at the wing root beneficially. Furthermore a key influence is the thrust which pre-stresses the wing structure. The results showed a suppression of several frequencies with lower amplitude to nearly vanish, whereas the dominant frequencies maintained in the frequency spectrum. As mentioned in the beginning the main question is the guarantee of safety during flight. Therefore an aerodynamic model needs to be implemented to investigate not only the structural coupling but the aeroelastic coupling behavior thus enabling a flutter simulation under consideration of the investigated influencial factors.

ACKNOWLEDGMENT

Financial support has been provided by the German Research Foundation (Deutsche Forschungsgemeinschaft, DFG) in the framework of the Collaborative Research Center 880.

COPYRIGHT STATEMENT

6 REFERENCES

[1] W. T. Feldt and G. Herrmann. Bending-torsional flutter of a cantilevered wing containing a tip mass and subjected to a transverse follower force. 297(6):467–478, 1974.

[2] F. H. Gern and L. Librescu. Effect of externally mounted stores on aeroelasticity of advanced swept cantilevered aircraft wings. (5):321–333, 1998.

[3] F. H. Gern and L. Librescu. Static and dynamic aeroelasticity of advanced aircraft wings carrying external stores. 36(7), 1998.

[4] M. Goland. The flutter of a uniform cantilever wing. 1945.

[5] I. Krukow and D. Dinkler. A reduced-order model for the investigation of the aeraeroelastic of circulation-controlled wings. *CEAS Aeronaut Journal*, 5(2):145–156, 2014.

[6] J. Kurzke. *GasTurb 12 - Design and Off-Design Performance of Gas Turbines*.

[7] I. Lottati. Aeroelastic stability characteristics of a composite swept wing with tip weights for an unrestrained vehicle. 24:793–802, 1987.

[8] T. S. Mueller and H. Hennings. Rotordynamic validation of a twin rotor-bearing system considering gyroscopic forces and bearing dynamics with a multibody formulation: Application to a geared uhbr gas turbine. In *DLRK*, 2016.

[9] R. Radespiel and W. Heinze. Sfb 880: Fundamentals of high lift for future commercial aircraft. *CEAS Aeronaut Journal*, 5(239-251), 2013.

[10] H. Rick. *Gasturbinen und Flugantriebe*. Spriner-Verlag, 2013.

[11] K. Sommerwerk, B. Michels, K. Lindhorst, M.C. Haupt, and P. Horst. Application of efficient surrogate modeling to aeroelastic analyses of an aircraft wing. 55:314–323, 2016.

[12] S. Waitz and H. Hennings. The aeroelastic impact of engine thrust and gyroscopics on aircraft flutter instabilities. *IFASD*, 2015.